11-2017

Characterization of Laser-Generated Aluminum Plasma Using Ion Time-of-Flight and Optical Emission Spectroscopy

Md. Haider A. Shaim
Old Dominion University

Hani E. Elsayed-Ali
Old Dominion University, helsayed@odu.edu

Original Publication Citation

Shaim, M. H. A., & Elsayed-Ali, H. E. (2017). Characterization of laser-generated aluminum plasma using ion time-of-flight and optical emission spectroscopy. *Journal of Applied Physics, 122*(20), 203301. doi:10.1063/1.4995477

Characterization of laser-generated aluminum plasma using ion time-of-flight and optical emission spectroscopy

Md. Haider A. Shaim, and Hani E. Elsayed-Ali

Citation: Journal of Applied Physics **122**, 203301 (2017);
View online: https://doi.org/10.1063/1.4995477
View Table of Contents: http://aip.scitation.org/toc/jap/122/20
Published by the American Institute of Physics

Characterization of laser-generated aluminum plasma using ion time-of-flight and optical emission spectroscopy

Md. Haider A. Shaim and Hani E. Elsayed-Ali[a)]
Department of Electrical and Computer Engineering and the Applied Research Center, Old Dominion University, Norfolk, Virginia 23529, USA

(Received 11 July 2017; accepted 31 October 2017; published online 22 November 2017)

Laser plasma generated by ablation of an Al target in vacuum is characterized by ion time-of-flight combined with optical emission spectroscopy. A Q-switched Nd:YAG laser (wavelength $\lambda = 1064$ nm, pulse width $\tau \sim 7$ ns, and fluence $F \leq 38$ J/cm^2) is used to ablate the Al target. Ion yield and energy distribution of each charge state are measured. Ions are accelerated according to their charge state by the double-layer potential developed at the plasma-vacuum interface. The ion energy distribution follows a shifted Coulomb-Boltzmann distribution. Optical emission spectroscopy of the Al plasma gives significantly lower plasma temperature than the ion temperature obtained from the ion time-of-flight, due to the difference in the temporal and spatial regions of the plasma plume probed by the two methods. Applying an external electric field in the plasma expansion region in a direction parallel to the plume expansion increases the line emission intensity. However, the plasma temperature and density, as measured by optical emission spectroscopy, remain unchanged. *Published by AIP Publishing*. https://doi.org/10.1063/1.4995477

I. INTRODUCTION

Laser ablation of a solid target results in the formation of dense plasma that is a source of multicharged ions (MCIs). The study of MCIs generation from laser plasma is a topic of interest because these MCIs provide valuable information on the laser-plasma characteristics in addition to their applications in ion implantation,[1] ion surface cleaning and patterning,[1] secondary ion mass-spectrometry,[2] extreme ultraviolet lithography,[3] and for injection in electron cyclotron resonance ion sources and ion accelerators.[4,5] Moreover, the ions generated by laser ablation impact thin film growth by pulsed laser deposition as these ions interact with the substrate.[6] The characterization of the different laser-generated ions involves measuring their number, charge state, energy distribution, and angular distribution. These measurements make use of a combination of different techniques such as time-of-flight (TOF) ion detection,[7] electrostatic retarding field analyzers,[8] and different configurations of electrostatic,[8] and magnetic[2] ion spectrometers based on ion bending.

Nanosecond (ns) lasers are often used to generate ions by ablation of a solid target in vacuum. During laser-matter interactions, the electromagnetic energy is converted into electronic excitation and then into thermal, chemical, and kinetic energies.[9] The process of ns laser ablation consists of three main stages: evaporation of the target material, interaction between the evaporated material and the laser pulse resulting in the formation of partially ionized vapor that absorbs the incident laser radiation, and plasma plume expansion and rapid cooling.[10] The laser energy is converted into internal energy of the plasma and emitted or absorbed during the hydrodynamic motion of the plume. Intense collisional ionization takes place in the hot plasma. Near the target surface, recombination releases energy acting against the adiabatic cooling, thus slowing down the recombination rate. Due to the rapid expansion of the plume, the plasma density is reduced before the recombination eliminates the ionized species, despite a rapid increase in the three-body recombination rate due to electron temperature decrease in the adiabatic expansion.[9] In the expanding plasma, different charge states become frozen. Hence, some of the MCIs generated in the hot plasma core survive and are ejected from the expanding plume.

In laser-plasma, three groups of ions have been reported, depending on the laser conditions.[9] The main group is composed of thermal ions that gain their energy from the thermalization processes followed by plasma expansion into the vacuum.[11] The fast ions are attributed to the presence of super-thermal electrons formed by the electrostatic waves.[12] The number of fast electrons is dependent on the laser intensity and wavelength.[12] Slow ion groups can be generated by secondary collisional processes during plume expansion or due to reabsorption of emitted x-rays outside the laser focus.[9,13,14]

Various processes have been proposed to explain the physical mechanisms of ion acceleration during ns laser ablation. The laser interaction with the plasma heats the plasma electrons by inverse bremsstrahlung. The energy of the heated electrons is then transferred to the neutrals and ions through collisions. The time needed to transfer the energy from the electrons to the ions, i.e., the electron-ion thermalization time scale (10^{-10} to 10^{-11} s),[15] is much shorter than the ns laser pulse duration resulting in the establishment of local thermal equilibrium (LTE) between the electrons and the ions during the early portion of the laser pulse.[15,16] Due to the mass differences between the electrons and the ions, fast electrons escape the plasma plume much earlier than the ions. The space-charge separation between the fast electrons and the ions that are lagging behind prevents some electrons from escaping the

[a)]Author to whom correspondence should be addressed: helsayed@odu.edu. Tel.: (757)269-5645.

plasma resulting in the establishment of a self-electrostatic field at the expanding plasma-vacuum interface. This field is referred to as the ambipolar electric field or the double-layer potential.[17] The ions, which enter in the region of this electric field, are accelerated according to their charge state.

Generation of a large number high-energy (hot) electrons during interaction of the laser pulse with the solid target and their subsequent escape from the expanding plume is the responsible mechanism for the formation of the double-layer potential. The hot electons are formed in the plasma by three-body recombination or absorption of the remaining laser pulse by inverse bremsstrahlung. Some of these hot electrons escape the target, leaving behind a positive electric charge region at the boundary of the expanding plasma-vacuum interface. The lifetime of the laser ablated plume is determined by the velocity of the plume expansion, which in turn is related to the hydrodynamic pressure inside the plume.[2]

The structure of the double-layer potential depends on the ratio of the hot electrons to thermal electrons, which is dependent on the laser fluence. With the increase in the laser fluence, more hot electrons are generated and the double-layer structure changes from a layer formed by the escaping electrons and the excess ions at the front of the expanding plasma core to a more complex two-peak structure with two double-layers.[17] The developed two-electron-distribution and the role of prompt electrons in the development of this complex double-layer structure was studied, both experimentally and by numerical simulations.[18] As the initial electron density at the front of the expanding plasma increases, electron compression in the plasma occurring by the forces of the prompt electrons, cannot be compensated for by the ion oscillation frequency. This results in ion cloud fragmentation and a complex ion acceleration mechanism.[18]

Ion emission for ns laser ablation was characterized by their TOF.[3,8,16,19–29] The charge state, kinetic energy, and angular distribution of the ions ejected from the laser plasma depend on the laser parameters (e.g., laser pulse energy, wavelength, and pulse duration), the ablated material, and the surrounding environment.[16] The general trend is that increasing the laser pulse energy increases ion generation. For example, laser ablation of carbon and aluminum with an Nd:YAG laser ($\lambda = 1.064\ \mu$m) showed enhancement of the ion generation along with the maximum charge observed with the increase in the laser pulse energy.[8,29] The effect of laser wavelength on the ion energy distribution from laser-ablated plasma in vacuum was studied. The ablation of a Sn target by a Nd:YAG laser ($\lambda = 1.064\ \mu$m) and by a CO_2 laser ($\lambda = 10.6\ \mu$m) yielded a maximum charge state of Sn^{6+} with an average ion energy of 792 eV for the Nd:YAG laser and Sn^{9+} with an average ion energy of 680 eV for the CO_2 laser.[19] A combined Langmuir probe and an electrostatic ion energy analyzer study of Al ions generated by a nanosecond Nd:YAG laser and a femtosecond (fs) Ti:sapphire laser at a comparable ablation flux yielded maximum charge state by the ns and fs lasers of Al^{2+} and Al^{3+}, respectively.[22] For the ns laser, the ions had a lower kinetic energy than that for the fs laser.[22] For a Pd laser ion source generated by a Q-switched Nd:YAG laser and its second harmonic, the ablation threshold was reported to be 1.2 times higher for $\lambda = 1064$ nm than for $\lambda = 532$ nm due to the longer penetration depth of the $\lambda = 1064$ nm in the metal.[20] For a laser pulse energy of 100 mJ, Pd^{5+} ions were detected for $\lambda = 1064$ nm, while Pd^{6+} ions were detected for $\lambda = 532$ nm.[20] The role of laser pulse duration on the ion emission from a Nd:YAG laser-generated Sn plasma was reported.[3] The ion kinetic energy profile shifted to higher energy with the reduction of the laser pulse width, while narrower energy distributions were obtained for the longest laser pulses used.[3] The average charge state decreased from Sn^{13+} to Sn^{7+} when the laser pulse duration was increased from 5 to 20 ns.[3] For ns laser ablation, Harilal reported that the plasma plume expands spherically with smaller laser spot size on target, while for a larger spot size, the plume propagation is more cylindrical due to the smaller lateral expansion.[21] Using a Faraday cup (FC) to study ion energy distribution, they showed narrower and higher energy ion distribution with the smaller spot size.[21] The dependence of the ion angular distribution on the laser parameters and the ablated material were reported by several groups.[23–28] The fs laser-ablated plume was more elongated along the direction normal to the target compared with that for ns laser ablation,[23] resulting in significantly narrower ion angular distribution at a similar laser fluence.[24] A narrower angular distribution of the plume occurs with increasing laser fluence.[25] Elsied *et al.* reported differences in the spatial and temporal distribution of slow and fast ions for various metals and related that observation to the different mechanisms in ion generation.[26] For Mo, the slow ion flux peaked at a direction normal to the target, whereas the fast ion flux peaked at relatively larger angles. For Al, the slow ions also peaked normal to the target while the fast ions were absent.[26] Torrisi *et al.*, utilizing a Nd:YAG laser, reported that the energy peaks of the singly-charged ions increases with the melting point of the ablated material, while the ablation yield showed the reverse trend.[27] Freeman *et al.* reported that the maximum kinetic energies of the ions generated by an Nd:YAG laser using its fundamental, second, and fourth harmonic with the same laser intensity were similar.[28] The kinetic energy distributions became broader as the laser wavelength was reduced, while the angular distribution of the ions showed a similar trend for all laser wavelengths.[28]

Several groups have studied ion emission from ns laser plasma using optical emission spectroscopy (OES).[7,10,30,31] Caridi *et al.* reported on ion generation by laser ablation of Al, Ti, Mo, Au, and polyethylene targets in vacuum using a Nd:YAG laser. For laser energy of 180 mJ, the electron temperature kT_e, obtained using optical emission spectroscopy, is ~1.3 eV, while the equivalent ion plasma temperature kT_i, as evaluated by TOF deconvolution using shifted Coulomb-Boltzmann (SCB) distribution, varies from 30 to 44 eV. The difference in plasma temperatures was attributed to the difference in the plasma region probed.[7] Abdellatif *et al.* studied Al plasma generated in vacuum by an Nd:YAG laser. The plasma density N_e was measured to be $1.13 \times 10^{18}\ cm^{-3}$ at a distance of 100 μm from the Al target surface and $0.55 \times 10^{18}\ cm^{-3}$ at 1200 μm from the surface. The measured T_e at the target surface was ~1.17 eV and increased to

4.2 eV 500 μm away from the surface, then it decreased beyond that point. Charge states up to Al^{+2} were observed.[30] Harilal *et al.* reported on OES studies of a Sn plasma generated in vacuum using a Nd:YAG laser. The kT_e and N_e measured 1 mm from the target surface were 3.2 eV and 7.7×10^{17} cm^{-3}, respectively.[10] The time-integrated kT_e near the target surface remained nearly constant with distance from the surface but increased significantly for a distance >7 mm.[10] The spatial variation of N_e showed approximately inverse dependence on distance. Applying a negative potential to a gold target was shown to increase ultraviolet line emission from the laser plasma produced by a KrF excimer laser, which was attributed to electric field enhanced recombination near the target surface.[31]

We extend our previous work on Al laser MCI generation[29,32] through a combined ion TOF measurement and OES of the laser plasma. The double-layer potential generated at the plasma-vacuum interface is estimated from the deconvolution of the TOF ion signal into individual ion species. From OES, the N_e is calculated by Stark broadening, while the kT_e is calculated using the relative intensity ratio of two emission lines belonging to the same atomic species. Although LTE is assumed valid for ablation conditions similar to ours,[33] the kT_i obtained from the deconvolution of the ion TOF signal is significantly higher than the electron temperature obtained from OES. This is attributed to the difference in time and location at which the plasma is probed. MCI generation occurs mainly when the plasma is at its highest temperature and at a high density near the surface and the core of the plume. Ions escaping from the plasma and accelerated by the double-layer potential reflect these conditions and therefore their TOF ion signal corresponds to the high temperature used to generate the ions, whereas OES probes time and spatially integrated line emissions, which becomes prominent after decay of the black-body radiation from the initial laser plasma. During this time, the plasma is providing strong line emission, the plume is expanding, and the plasma is cooling. Therefore, the spatially and temporally integrated line emission, as detected by the spectrometer, provides a much cooler electron temperature. The peak intensity of the spectral lines and the ion energy spread show dependence on the external electric field in which the plume expands.

II. EXPERIMENTAL

The laser ion source is composed of a Q-switched Nd:YAG laser ($\lambda = 1064$ nm, $\tau \sim 7$ ns, and laser fluence $F \leq 38$ J/cm^2) with associated laser beam delivery optics, target ablation chamber, ion drift tube, three-grid retarding field ion energy analyzer, and Faraday cup (FC). The laser was *p*-polarized and incident on the target at an angle $\theta = 45°$. The laser was focused on the target using a lens with 80 cm focal length. The laser pulses pass to the Al target through a viewport which has ~8% loss due to Fresnel reflections. The laser was focused on the Al target forming an elliptical spot (semi major axis radius 0.3 mm, and semi minor axis radius 0.25 mm) with an area of ~0.0024 cm^2. A fast high voltage probe (Tektronix P6015A) is used to observe the voltage fluctuations of the biased target during plasma plume expansion. The currents flowing through the Al target and the externally grounded extraction mesh are measured separately using two current pickup coils (Pearson current monitor, model 4118). The pressure in the vacuum chamber was maintained at low 10^{-9} Torr.

The ions are accelerated towards the FC through a drift tube. The diameter of the MCI generation vacuum chamber is 30 cm. A 125-cm long transport tube with inner diameter of 10 cm is connected to the MCI generation chamber making the distance from the Al target to the FC 140 cm. The FC biased at −70 V detects the TOF ion signal, which is used to calculate the total charge delivered to the FC and their kinetic energy. The TOF signal can be used to identify the charge state of the ions generated. The ion signal is acquired by a fast-digital oscilloscope triggered by a photodetector observing the optical leak in the last mirror before the focusing lens. An illustration of the experimental setup is shown in Fig. 1. More details on the experimental setup for ion generation and detection are given in our previous publications.[29,34,35]

To further accelerate the extracted ions, the target is biased positively while a grounded mesh is placed in front of it. The extraction mesh is placed at 10 cm away from the Al target towards the FC, where the density of the plasma is several orders of magnitude lower than at the target surface. The plasma plume expands in the electric field generated between the target and the grounded mesh. The adiabatic expansion, thermal interactions, and the Coulomb acceleration due to the double-layer potential at the plasma-vacuum interface are mainly responsible for the initial ion acceleration. The external electric field accelerates ions separated from the plume. The ion acceleration by the external electric field is reduced due to plasma shielding. The location between the target and the grounded mesh at which an ion experiences the electric field also affects the ion acceleration by the external electric field. The ion flux extracted increases with the electric field due to the retrograde motion of the plasma edge exposing more ions to the accelerating field and repelling the electrons.[36] In the drift region, the temporal ion pulse width is increased.

An optical spectrometer [Princeton Instruments, Acton SP2300 (grating size 68 × 68 mm, 150 grooves/mm, blaze wavelength 500 nm, and a resolution of 1.27 nm as provided

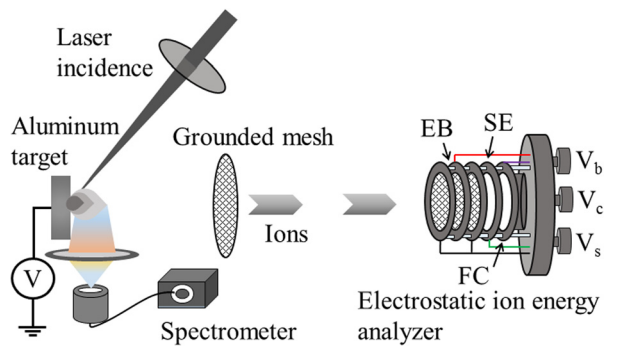

FIG. 1. Schematic of the experimental setup, EB denotes the electrostatic barrier of the three-grid retarding field analyzer, and SE the suppressor electrode to suppress the effect of secondary emission from the Faraday cup (FC).

by the manufacturer)] is used to obtain the optical spectra from the laser plasma. The optical spectra were collected for 1 ms using a single-shot mode and without any set delay between capturing the optical spectra and the laser pulse. The emission from the formed plasma is imaged onto the open end of an optical fiber bundle using a lens of 5 cm diameter with a focus length of 5 cm. The optical fiber bundle has 19 optical fibers, each 200 μm in diameter and 1 m long with a numerical aperture of 0.2. The spectra were observed in a direction parallel to the target surface (i.e., 90° with respect to the direction of the plasma expansion) with its axis centered ~1 mm from the surface of the sample and the fiber is placed ~250 mm away from the produced plasma. The position of the fiber is far enough to obtain spatially-integrated spectra from the plasma. The spatially-integrated, time-integrated spectra from each pulse are detected, and the final spectra used in the analysis were an average of 10 laser pulses. For a similar experimental condition, the plasma emitting region is >5 mm above the sample surface.[37]

III. RESULTS

A. Effect of laser energy for a grounded target

Figure 2 shows the TOF ion signal for laser fluence of 21, 25, 28, and 38 J/cm^2. The inset of Fig. 2 shows that the total number of charge generated increases linearly with the increase in the laser fluence. The ion pulse that reaches the FC contains different ionic states. The double-layer potential, developed at the expanding plasma-vacuum interface, accelerates the ions. Higher charge state ions reach the FC earlier than those with a lower charge, since the ions with higher charge gain more kinetic energy by the double-layer potential. From analysis of the shape of the ion signal, we show that, with the increase in the laser fluence, the ion energy distribution shifts to higher energies along with the generation of higher charge-state ions. Increasing the laser fluence from 21 to 38 J/cm^2 increases the peak ion drift velocity from ~1.9×10^4 to ~2.4×10^4 ms^{-1}, resulting in a peak ion energy increase from ~50 to ~80 eV.

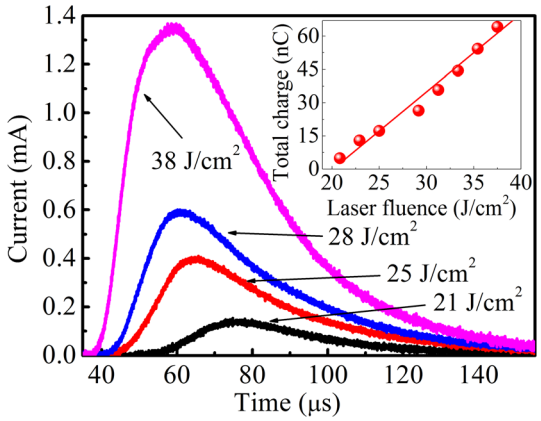

FIG. 2. Ion TOF signal for different laser energies ablating the Al target. The Al target was at ground potential. The inset shows the dependence of the number of charge measured by the Faraday cup (FC) on the laser pulse energy.

The ion energy distribution can be used to characterize the plasma temperature and the double-layer potential developed at the plasma-vacuum interface of the expanding plume. The ion TOF signal is detected by the FC. The ion TOF signal and the retarding field energy analyzer are used to obtain the ion energy distribution. The TOF signal can be deconvoluted into individual ion charge signals. For a transient laser-plasma satisfying LTE ($T_i \sim T_e \sim T$), the electron-atom and electron-ion collisions establishes equilibrium with the particle velocities in the plasma following a Maxwell-Boltzmann distribution.[10] The validity of the LTE for ns laser plasma was previously considered.[33] Accordingly, our plasma conditions satisfy LTE. Away from the target, where recombination and collisional excitation processes are absent, the ion charge-states are frozen and the ions drift freely in the vacuum with a velocity distribution for each ion species characterized by a shifted Coulomb-Boltzmann (SCB) distribution.[16] For a laser-plasma where the TOF of the extracted ions is much longer than the laser pulse duration, the Kelley and Dreyfus function expressing the ion current based on the SCB distribution, including the effect of Coulomb energy (in terms of an equivalent accelerating voltage) can be applied for the analysis of the ion current.[38,39] Both thermal and Coulomb interactions are considered in the SCB model. Therefore, the sum of the individual SCB distributions for each ion species with their characteristic equivalent accelerating voltage and ion plasma temperature provides the overall distribution of the ejected ions[7]

$$F_{(t)} = \sum_i A_i \left(\frac{m}{2\pi k T_i}\right)^{\frac{3}{2}} \left(\frac{L^4}{t^5}\right) \exp \times \left[-\frac{m}{2kT_i}\left(\frac{L}{t} - \sqrt{\frac{\gamma k T_i}{m}} - \sqrt{\frac{2zeV_{0,i}}{m}}\right)^2\right], \quad (1)$$

where A_i are normalization constants, m is the mass of the ablated ions, t is the time-of-flight, and L is the total distance from the target to the Faraday cup. $v = \frac{L}{t}$ is the velocity along the normal to the target and is equal to the summation of the velocity components v_t, v_k, and v_c. The component $v_t = \sqrt{\left(\frac{3kT_i}{m}\right)}$ is the mean thermal velocity for monoatomic neutral species, $v_k = \sqrt{\frac{\Upsilon k T_i}{m}}$ is the adiabatic expansion velocity, and $v_c = \sqrt{\frac{2zeV_0}{m}}$ is the velocity due to Coulomb acceleration. In the velocity components, Υ is the adiabatic coefficient which for a monoatomic metal, e.g., aluminum, has the value of 5/3, z is the charge state, kT_i is describes the velocity spread of the probed ions, which has been assumed equivalent to the ion plasma temperature (in eV) in previous laser MCI studies,[7,16] and V_0 is the equivalent accelerating voltage developed at the plasma-vacuum interface. Equation (1) applies under the condition of the absence of significant recombination and collisional excitation processes, i.e., the ion species are frozen and freely drifting in the vacuum.[40] The curve fit of the TOF signal with Eq. (1) mostly depends on the kT_i and V_0 developed at the plasma-vacuum interface due to the double-layer potential. We can estimate kT_i and V_0 from the curve fit of the measured TOF signal with Eq. (1).

The ion pulse detected by the FC, shown in Fig. 2, consists of ions with different charge states. To determine the contribution of each ion charge to the TOF signal, deconvolution of the ion pulse signal for each ion charge state is accomplished. The best fit to the TOF signal is obtained for a combination of kT_i and V_0 developed in the double-layer region of the plume. These two parameters can be used to estimate the effects of thermal energy, adiabatic expansion, and Coulomb potential on the energy distribution of the individual ion species. The deconvolution of the ion pulse into individual ion species is conducted as follows: first, we fix the value of the maximum charge state n (known by separating the charge states temporally using an externally applied electric field between the target and the grounded mesh). Then, we set the V_0 and the kT_i as free variables to bring the total energy (sum of thermal, adiabatic, and Coulomb) to match with the ion pulse suppression potential applied to the central grid of the three-grid retarding field analyzer. Other conditions used for the fit are that the sum of the TOF de-convoluted signals of individual ion species fits with the measured TOF signal of the detected ion pulse. Also, the ratio of the ion charges detected for each charge state matches with that ratio as measured when an external electric field is used to separate signals from each charge state by their TOF. The details of the deconvolution procedure were given previously.[29]

Previous ion TOF studies from ns laser plasma have shown that the ion energy distribution, for a certain ion charge, splits into two SCB distributions peaked at different energies.[13,14] Bimodal energy distributions for metal ions at different peak energies were reported for ablation with a ns Nd:YAG laser. The SCB distribution of Al^{1+} ions with the higher velocity was correlated with the direct multiphoton laser ionization, while the slower distribution was associated with collisional processes. In the expanding plume, neutrals can be ionized and ions can be converted into another charge state due to the collisions among ions, electrons, and neutrals leading to ionization, recombination, and ion charge transfer. Ions produced due to collisions have velocities that depend on their formation process and hence are observed as an independent energy distribution.[13,14] The external energy gain also depends on the location between the target and grounded mesh, where the ion is generated, and the distance the ions travelled experiencing the external electric field. Ion acceleration by the external electric field is reduced due to plasma shielding. For example, if electron-impact ionization is the dominant process $(Al^0 + e^- \rightarrow Al^+ + 2e^-)$, the kinetic energy of the Al^0 involved in this reaction will contribute to the energy distribution of the resulting Al^{1+} ions. Recent studies of ns laser ablation observed the presence of fast and thermal ions following Gaussian and Maxwell-Boltzmann distributions, respectively.[26] The presence of fast ions depends on the atomic weight of the ablated material. For heavy metals, e.g., Mo, fast and thermal ions were observed. While for lighter metals, e.g., Al, only thermal ions were detected.[26] This phenomenon was attributed to the difference in both spatial and temporal ion distributions along with the fact that ns laser ablation of heavy metals emits prompt electrons, and these prompts electrons are responsible for the emission and acceleration of the fast ions. Similar results for ns laser ablation were reported by Farid *et al.*, where higher Z materials (Mo, T, and W) show multiple peaks containing fast and thermal ions, while lower Z materials (C, Al, Si, and Cu) show only a single peak containg thermal ions.[41] In our present experiment with Al, no fast ions were detected; only thermal and slows ions are detected and are fitted with SCB distribution.

The deconvolution of the ion pulse into individual ion species for laser fluence of 28 and 38 J/cm^2 is shown in Figs. 3(a) and 3(b). The higher charge state ions have higher velocities and, therefore, reach the FC earlier than the lower charge states. The sum of the signals from different ion charges gives the total ion signal, which is fitted to the experimental TOF signal. The ions generated with laser at a fluence of 28 and 38 J/cm^2 have energies up to ~70 and ~80 eV, respectively, as measured by the retarding field analyzer.[29] During retarding field analysis, the barrier voltage, applied to the central electrode of the three-mesh retarding field analyzer, was increased from 0 to 80 V. From the deconvolution, we obtain charge states up to Al^{3+} and Al^{4+} when the laser fluence is 28 and 38 J/cm^2, respectively. This is confirmed by observing the individual ion peaks for each charge in the TOF signal when voltage is applied to the target setting an external electric field sufficient to separate the different charge states.

The curve fit in Fig. 3(a) was done for $V_0 = 50$ V and $kT_i = 9$ eV and in Fig. 3(b) for $V_0 = 55$ V and $kT_i = 10$ eV. The slow ions Al_s^{1+} are fitted with $V_{0S} = 20$ V with similar kT_i as used to fit the thermal ions. For laser fluences of 21 and 25 J/cm^2 (data not shown), the best fit to the TOF signal gave $V_0 = 35$ and 43 V and $kT_i = 6$ and 8 eV, respectively, while V_{0S} was 15 V for both laser fluences. Other slow ion

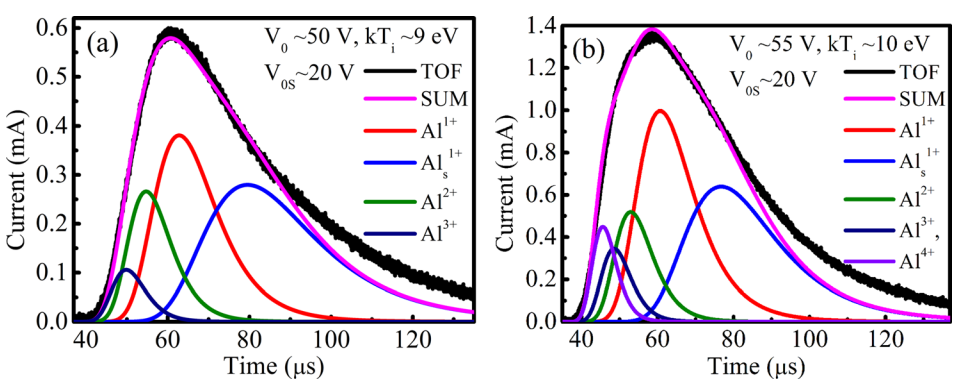

FIG. 3. Deconvolution of the ion time-of-flight signal. (a) For a laser fluence of 28 J/cm^2 showing charge states up to Al^{3+}. (b) For a laser fluence of 38 J/cm^2 showing charge states up to Al^{4+}. V_0 is the double-layer potential, kT_i is the ion plasma temperature, whereas V_{0S} is the equivalent accelerating voltage for the slow Al^{1+} ions.

groups could also affect the ion TOF signal. With the target grounded, for an ion with charge state z, the total energy gain of the ion $E_{zT} = (E_t + E_k) + zE_C$, where $E_t = \frac{3}{2}kT_i$ is the thermal energy, $E_k = \frac{\gamma}{2}kT_i$ is the adiabatic energy, and $E_c = eV_0$ is the Coulomb energy associated with the equivalent accelerating voltage due to the double-layer potential. The most probable energy calculated from the TOF signal, and the adiabatic and thermal energy estimated from the deconvolution of the TOF signal are in good qualitative agreement with the results previously reported from ns laser ablation.[42] This fit is best at time scales extending from the onset of detecting the thermal ions by the FC and extends past the peak of the TOF signal. The slower ions forming the tail of the TOF signal are not as well fitted to the SCB distribution, representing the sum of the ion charges. This is because there are secondary mechanisms forming these slower ions, as was previously discussed.[13,14]

B. Effect of laser energy for positively biased target

When the target is positively biased establishing an electric field between the target and the grounded mesh, the ions that separate from the plume experience further acceleration. For sufficient acceleration, the ions detected by the FC appear as temporally separated peaks for each charge state. The extent of which the ions experience the external field depends on the distance away from the target that they are separated from the shielding plasma. If an ion is generated with zero energy near the target and is accelerated by the full potential applied, i.e., in the absence of plasma shielding, the ions TOF to the FC is $TOF = t_a + t_d = \sqrt{\frac{2m}{zeV}}d + \sqrt{\frac{m}{2zeV}}S$, where t_a is time to accelerate the ions in the extraction region, t_d is the ions drift time from the extraction mesh to FC, d is the length of the extraction region, S is the length of the drift region, i.e., from the grounded mesh to FC, m is the mass of Al atom, e is the electron charge, z is the charge state, and V is the external potential applied. This TOF equation does not account for the ion acceleration experienced by the double-layer potential, and due to the adiabatic and thermal expansion of the plume. The ions travel time in the extraction region is much smaller than the drift time. The effective acceleration experienced by the ions depends on the traveled distance of the plasma before the ions are extracted. Each ion charge state is accelerated in the double-layer potential region and by the external field according to the charge state. Al^{1+} gains the least energy compared to higher charge states and, therefore, has the lowest velocity and its TOF is the longest. By calculating the accelerating potential required to achieve the TOF of Al^{1+}, the effective accelerating potential that the Al^{1+} experience is obtained. This potential is then used to determine the TOF of ions with higher charge states. The estimated TOF for Al ions with different charge states matches the experimental TOF signal well. By adding the effective external potential V_{eff} with the double-layer potential V_0, we can further extend the SCB distribution. To do so, we replaced the V_0 term in Eq. (1) with total accelerating voltage $V_T = (V_0 + V_{eff})$. This results in ion pulses with peaks that are temporally separated with each pulse corresponding to a different charge state. The sum of these separated pulses is the signal observed by the FC. From the peak of the TOF signal of each charge state, the most probable energy can be calculated. The total energy of the ions with charge state z is equal to the sum of the ablation energy (sum of thermal and adiabatic expansion), Coulomb energy (from double-layer potential), and the effective accelerating voltage and can be written as $E_{z-Total} = E_T + E_K + zE_c + zE_{eff}$, where E_{eff} is the effective acceleration energy experienced by the ion from the external electric field. The value of E_{eff} is less than the voltage applied to the target due to the plasma shielding and secondary ion generation mechanism in the target-to-extraction grid region.

As the ions drift in the external electric field, they experience different acceleration by the external electric field depending on their generation location and the dynamics of plasma shielding in addition to the retrograde motion of the plan separating the neutral plasma from the non-neutral region established by the double-layer potential.[17,36] The plasma expansion dynamics in an external electric field is complex and has been the subject of a few studies.[43] When the plasma expands in a field-free region, kT_i can be deduced from the fit of the ion signal, far away from the ablation point, as was shown in many publications.[7,16,40] However, when the plasma expands in an external electric field, obtaining kT_i from the SCB fit is problematic as the width of the TOF signal is affected by additional mechanisms occurring in the region between the target and the grounded grid causing ions with similar charge to experience slightly different electric field, thus broadening the ion pulse. In this case, the TOF fit to the SCB distribution would not give an accurate kT_i of the ablated plume but rather a higher value that represents the spread in the kinetic energy of the detected ions as a result of their plasma ion energy and the complex plume and ion extraction dynamics in the target-grid region for an external applied field. Therefore, we refer to this parameter used in the fit as the effective ion energy spread due to the combined plasma ion temperature and ion energy spread in the external electric field and refer to this quantity as kT_{ie} which is larger than the kT_i used for the SCB fit under plume expansion without an external field.

Figure 4 shows the deconvolution of the ion signal into different ion charges for 5 kV applied to the target. When the laser fluence is 28 J/cm^2, the ratio of the ion charges Al^{1+}:Al^{2+}:Al^{3+} is ~6.2:3:1, and for a laser fluence of 38 J/cm^2, this ratio for Al^{1+}:Al^{2+}:Al^{3+}:Al^{4+} is ~6:1.6:1:1. The deconvolution of the TOF signal for a laser fluence of 28 J/cm^2 yielded total accelerating voltage $V_T \sim 1.55$ kV and kT_{ie} ~26 eV. The increase in kT_{ie} with the applied voltage to the target reflects the spread in the energy of the ions probed by their TOF due to the dynamic nature of the plasma expansion in an external electric field. The external electric field is mostly shielded from the expanding plasma and would not cause plasma heating. When the laser fluence was 38 J/cm^2, as shown in Fig. 4(b), the deconvolution yielded total accelerating voltage $V_T \sim 1.6$ kV and $kT_{ie} \sim 27$ eV. The deconvolution of Figs. 4(a) and 4(b) also shows the presence of slow

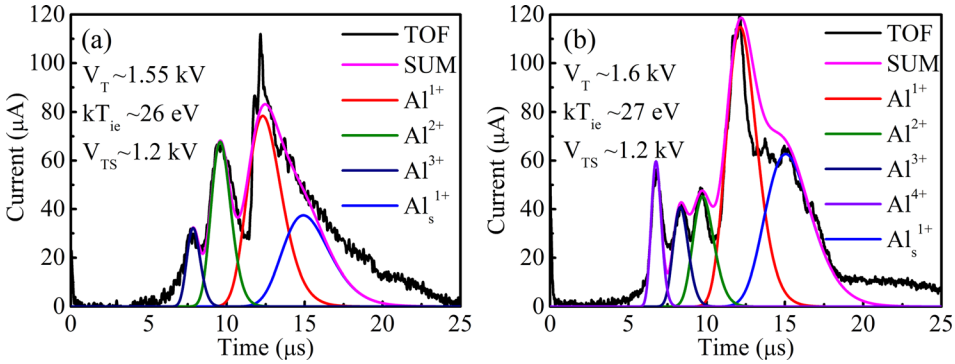

FIG. 4. Deconvolution of the TOF signal for different ion charge states for 5 kV applied to target. The laser fluence is (a) 28 J/cm^2 and 38 J/cm^2 (b). V_T is the total effective voltage accelerating the ions and kT_{ie} represents the spread in ion energy due to the plasma ion temperature and ion spread during plume expansion and ion extraction in the target-grid region, and V_{TS} is the effective accelerating voltage for the slow ions.

Al^{1+}. The slow ions were fitted for $V_{TS} = (V_{0S} + V_{eff})$ ~1.2 kV.

The sensitivity of the deconvolution is checked by varying the values of z, V_T, and kT_{ie}. Figure 5 shows the fit performed for Al^{4+} using different V_T and kT_{ie} values. kT_{ie} determines the ion pulse width for each charge state irrespective of the external electric field. V_0 determines the ion pulse energy shift by the Coulomb energy associated with the double-layer potential, while $V_T = (V_0 + V_{eff})$ adds the effect of the external electric field. The effect of V_T on the fit is more dominant than that for kT_{ie} and, for higher charge ions, the sensitivity of the fit to the value of V_T is higher. If kT_{ie} is kept constant, the energy shift in the SCB distribution is determined by V_T, whereas for a fixed V_T, kT_{ie} mainly determines the ion pulse width. As shown in Fig. 5, 300 V change in V_T shifts the Al^{4+} ion most probable energy by 1200 eV. Changes in kT_{ie} by 13 eV mostly affect the ion pulse width. For higher charge states, the accuracy of the fitting parameter V_T increases.

C. Effect of target bias voltage

Figure 6 shows the deconvolution of the ion TOF signal for 4 and 6 kV applied to the target when a laser fluence of 28 J/cm^2 is used to ablate the target. The amplitude of the ion signal increases with the increase of the electric field between the Al target and the grounded mesh. For an acceleration voltage of 4, 5, and 6 kV, with all other conditions fixed, the total charge detected was 0.25, 0.5, and 0.65 nC, respectively. The ratio of the different ion charges detected remains nearly the same for the different target bias voltages. This indicates that changes in the external electric field between the target and mesh for our experimental conditions have negligible effect on the angular distribution of the detected ions. The applied electric field introduces retrograde motion of the expanding plasma edge exposing more ions to the accelerating field and repelling the electrons.[36] This is thought to be the main reason for the enhancement of the ion extraction with increasing electric field between the Al target and the extraction grounded mesh. In Fig. 6(a), when 4 kV is applied to the target, the ion TOF signal has a best fit for $V_T \sim 1100$ V and $kT_{ie} \sim 20$ eV. When 6 kV is applied to the target, the best fit to the ion TOF signal is obtained for $V_T \sim 1900$ V and $kT_{ie} \sim 30$ eV, as shown in Fig. 6(b). The deconvolution in Figs. 6(a) and 6(b) also shows a low energy tail in the ion TOF signal due to slow Al^{1+}. For 4 and 6 kV accelerating voltage, the TOF signal for the slow ions is fitted for V_{TS} of ~800 and ~1400 V, respectively. The insets of Figs. 6(a) and 6(b) show the energy distribution of the ions as obtained from the ion TOF signal. The initial bumps present in the energy distribution are due to the slow energetic ions. The ion energy spread, $\frac{\Delta E}{E}$, is dependent on the charge state, and is ~42% for Al^{1+}, ~32% for Al^{2+}, and ~25% for Al^{3+}. This resolution is not affected by the target biasing voltage.

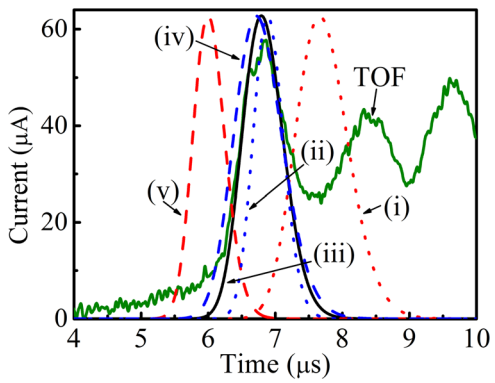

FIG. 5. The effect of varying the total accelerating voltage V_T and kT_{ie} on the deconvolution of the ion pulse when 5 kV accelerating voltage is applied. The Al^{4+} ion pulse obtained by deconvolution is shown for (i) $V_T \sim 1300$ V and $kT_{ie} \sim 27$ eV (red dotted line), (ii) 1600 V and 14 eV (blue dotted line), (iii) 1600 V and 27 eV (black straight line), (iv) 1600 V and 40 eV (blue dashed line), and (v) 1900 V and 27 eV (red dashed line).

D. Retarding field ion energy analysis

To characterize the ions from the laser plasma, the voltage applied to the electrostatic barrier (EB) mesh was incrementally increased from 0 V to a voltage that resulted in complete suppression of the ions detected. The laser fluence of 28 J/cm^2 was used to ablate the Al target, while 5 kV was applied to the target. Figure 7 shows the TOF signal for 0, 0.6, 1.2, 1.8, 2.0, and 2.4 kV applied to the EB. The inset of Fig. 7 shows the reduction in the total number of charges reaching the FC with the increase in the EB voltage. Higher charge state ions reach the FC earlier than those with a lower charge since the ions gain kinetic energy from the double-layer potential and from the external electric field, proportional to their ion charge. The EB potential V_{EB} suppresses all ions having kinetic energy lower than zeV_{EB}. From Fig. 7, we observe that the EB bias of 1.8 kV suppresses more than ~80% of the Al ions. The ion energy measured from the EB,

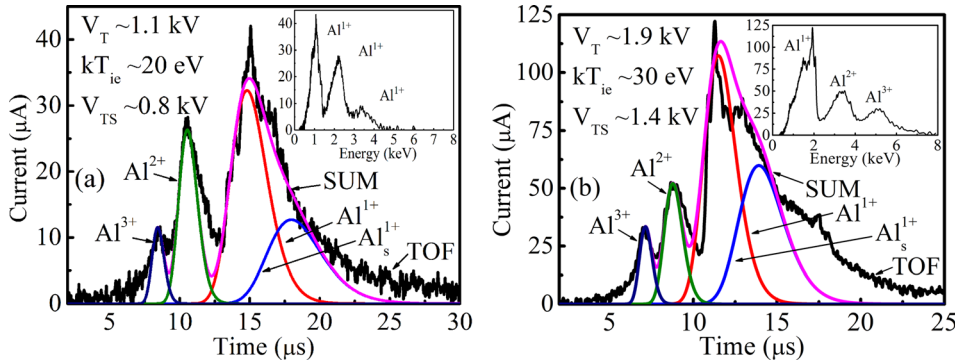

FIG. 6. Deconvolution of the ion TOF signal into different charge states for a voltage applied to target of (a) 4 kV and (b) 6 kV. The ablating laser fluence is 28 J/cm^2. The TOF signal is plotted in black. The deconvolution fit for Al^{1+}, Al^{2+}, Al^{3+}, and Al_s^{1+} are plotted in red, green, navy, and blue, respectively. The sum of the individual de-convoluted ion species is plotted in pink. Inset shows the TOF signal converted into energy distribution of the ions.

TOF signal, and the deconvolution of the TOF signal are in good qualitative agreement.

E. Optical emission spectroscopy

We use the optical spectra of the laser plasma to estimate the kT_e and N_e. The emission spectra captured is time-integrated but limited to the plasma observation location, which restricts the observation time depending on the plume expansion velocity. The plasma is moving in a direction perpendicular to the target surface. In our experiment, the fiber used has an acceptance angle of ~11°. The lens that image the plume on the fiber optics bundle input is set to image the plume at and near the surface of the target. We estimate that optical emission from a distance up to ~3 cm from the target is captured by the spectrometer. According to Harilal *et al.*,[44] for Al ablation with nearly the same laser parameters, the plume has an expansion velocity of $>10^7$ cm s^{-1}. With this velocity, the plume takes less than 300 ns to pass the region imaged on by the fiber bundle connected to the spectrometer. For a ns laser ablation of Al by Nd:YAG laser in vacuum, Freeman *et al*. reported that the electron density and temperature measurement for time up to ~450 ns after the laser ablation satisfying the LTE condition.[33] Figure 8 shows the optical spectra when the Al target is ablated by a laser fluence of 21 J/cm^2 without and with a voltage of 7 kV applied to the target. The NIST database is used to identify the atomic and ionic emission lines.[45] Line emission due to neutrals and ions with charge states up to Al^{2+} are detected. The external electric field affects both the atomic and ionic spectral lines. There is a clear enhancement in the intensity of the spectral lines (both atomic and ionic) in the presence of an external electric field. The enhancement of the optical emission line intensities and the background is due to the shorting of the biased Al target to the grounded mesh, placed in front of the target, by the expanding plume. This shorting results in current flow from the power supply through the target and the plasma to the grounded grid. This current flowing between the biased Al target and grounded mesh is detected by a current pick-up coil detecting the current flow out of the grounded mesh. The current through the grounded mesh starts flowing at ~1 μs after the ablating laser pulse and is sustain for another ~1 μs corresponding to the time this glow discharge between the target and grid is extinguished as the plume passes that region. We believe that increased optical emission and its detection time are responsible for the increase in the integrated intensity in Fig. 8 when an external field is applied. In addition to enhancing the Al line emission intensity, a new emission line corresponding to the Ni I at

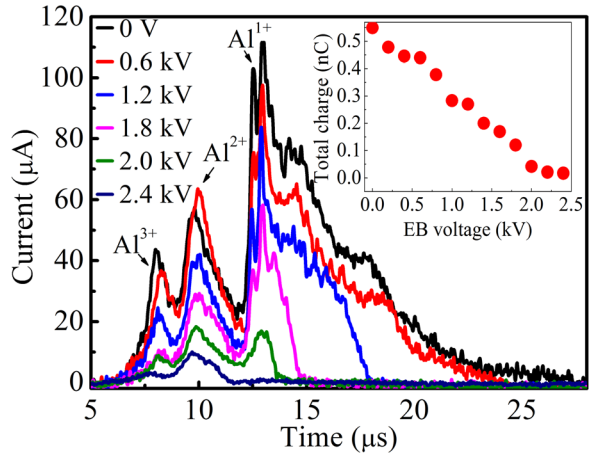

FIG. 7. Effect of retarding voltage on the TOF spectrum for a laser fluence of 28 J/cm^2 and 5 kV applied to target.

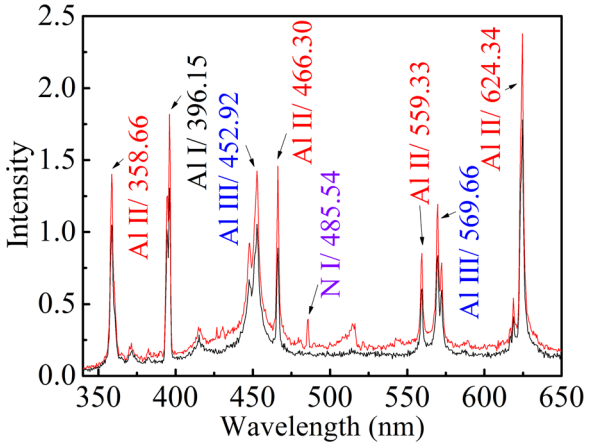

FIG. 8. Al emission spectra for laser fluence of 21 J/cm^2, when no external electric field (black line) and when 7 kV external field (red line) is applied.

485.54 is detected when the target is biased at 5 and 7 kV. This line is probably due to the sputtering of Ni grounded mesh, placed in front of the target, which acts as the cathode of the discharge between the target and mesh. While sputtering of the Ni mesh by the laser-generated ions would also occur without target bias, its rate will be significantly less due to the lower ion energy. As the optical detection geometry detects only a distance up to ~3 cm from the target, Ni lines will only be detected if Ni is present in that region during the discharge established between the target and the Ni grid.

For optically thin plasma, Stark broadening of line emission from neutrals or singly charged ions is used to estimate the N_e.[46] Applying the procedure described by Radziemski *et al.*, for Al II lines at 704.21 and 705.66 nm, the statistical weight of the upper level of the lines are found proportional to the intensity ratio of the lines; therefore, the plasma was optically thin and stark broadening analysis can be applied.[47] In the present experiment, the Stark-broadened profile of the Al II line at 466.30 nm [$4p^1P^0(1)$–$3p^2D(1)$] was used after fitting the line-shape to a Lorentzian profile, because of a comparatively lower self-absorption coefficient.[48] Three main broadening mechanisms contribute to line broadening, namely, Doppler broadening, resonance pressure broadening, and Stark broadening. For laser plasma similar to ours, the effect of Doppler broadening and resonance broadening is very small compared to Stark broadening and can be neglected.[49] The mechanism causing Stark broadening of the Al II transitions is mainly due to perturbation of the energy levels of the ions by electron collisions leading to broadening of the emission lines. The instrumental response was obtained by fitting the line-shape of the 404.65 nm line from a low-pressure Hg lamp to a Lorentzian profile and was found to be 0.7 nm. This instrumental response was subtracted from the experimental linewidth of the Al II line at 466.30 nm. Equation (2) can be used to correlate the full-width at half-maximum (FWHM) of the Stark-broadened line $\Delta\lambda_{1/2}$ with the N_e[50]

$$\Delta\lambda_{1/2} = 2\omega\left(\frac{N_e}{10^{16}}\right) + 3.5A\left(\frac{N_e}{10^{16}}\right)^{\frac{1}{4}} \times \left(1 - 1.2{N_D}^{-1/3}\right)\omega\left(\frac{N_e}{10^{16}}\right)\text{Å}, \quad (2)$$

where ω is the stark broadening parameter, and for Al II line at 466.30 nm, it has a value of 0.0538 nm at a temperature of 15 000 K,[50] A is the ion broadening parameter. Both ω and A are weak functions of temperature.[46] N_e is the electron density in cm^{-3} and N_D is the number of particles inside the Debye sphere. The first term of the Eq. (2) accounts for the electron broadening, and the second term is the correction for the quasi-static ion broadening. The quasi-static ion broadening term is small in plasma, similar to our case as was estimated from the extrapolation of the estimates of ω and A.[46,49] Therefore, Eq. (2) becomes

$$\Delta\lambda_{1/2} = 2\omega\left(\frac{N_e}{10^{16}}\right)\text{Å}. \quad (3)$$

To determine the kT_e, we use the line emission intensity analysis. This method can be applied when the plasma satisfies LTE and is applicable to our laser plasma conditions, as described in previous studies using similar lasers.[33] The excitation temperature can be determined using the following equation:[46]

$$T_e = \frac{E_2 - E_1}{k}\left[\ln\left(\frac{I_1\lambda_1 g_2 A_2}{I_2\lambda_2 g_1 A_1}\right)\right]^{-1}, \quad (4)$$

where k is the Boltzmann constant, E_2 and E_1 are the energies of upper transition levels of two lines utilized for electron temperature estimation and belong to the same atomic species. I_1, A_1, g_1, and λ_1 are total intensity (integrated over the line profile), transition probability, degeneracy, and wavelength of the line with upper level E_1, respectively. The subscript 2 refers to the line with upper level E_2 for the corresponding quantities. Al II lines at 358.66, 466.30, 559.33, and 624.34 nm are used to calculate the plasma kT_e. Figure 9 shows the N_e (a) and kT_e (b) with the increase in voltage applied to the target for laser fluence of 21–38 J/cm^2. In Fig. 9(b), the average kT_e is plotted with the error bar representing the maximum and minimum values obtained from the line emission analysis. We observe that the N_e and kT_e increase significantly with the increase of laser fluence, but shows no change, within the experimental error, with the applied external electric field.

Using the value of N_e and kT_e in the McWhirter criterion, we can determine whether the generated plasma satisfy the LTE condition. To satisfy the LTE condition, the lower limit of the N_e has to fulfill the following condition:[30]

$$N_e(\text{cm}^{-3}) \geq 1.6 \times 10^{12}[T_e(K)]^{\frac{1}{2}}[\Delta E(\text{eV})]^3, \quad (5)$$

where ΔE is the largest energy transition from which the condition holds, and for our case, it is 3.65 eV, and T_e is the plasma temperature.[30] The plasma temperature we obtained for a laser fluence of 21 J/cm^2 when no accelerating voltage is applied is ~1.1 eV. Accordingly, the lower limit of N_e for

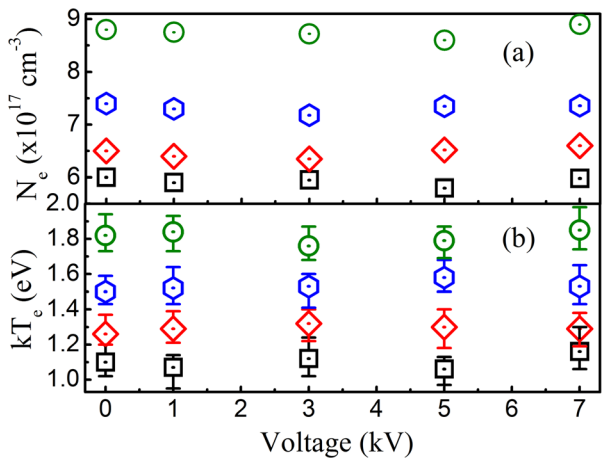

FIG. 9. Effect of target bias voltage on (a) electron density N_e and (b) electron temperature kT_e as measured by OES. Laser pulse energy of 21, 25, 28, and 38 J/cm^2 is represented by black-square, red-diamond, blue-hexagon, and green-circle, respectively.

the LTE condition using Eq. (5) is $8.8 \times 10^{15}\,\mathrm{cm}^{-3}$. The N_e value we obtained using OES is greater than the minimum LTE condition value leading to the conclusion that LTE is applicable to the studied plasma.

For laser fluence range from 21 to 38 J/cm^2, kT_i of the ejected ions evaluated by the TOF deconvolution varied between ~6 to ~10 eV when no accelerating voltage is applied, while when up to 6 kV accelerating voltage is applied kT_{ie} ranges from ~20 to ~30 eV, whereas the kT_e calculated from the optical spectra varied between ~1.1 to ~1.8 eV for the same laser fluences. Without an applied external field, the difference in the values of kT_i measured by ion TOF and kT_e measured by OES is attributed to the difference in time and location at which the plasma is probed. For ns laser pulse ablation, plasma reaches its highest temperature during the laser pulse with its highest density near the surface forming the core of the plasma, and therefore, the ions are generated during the laser pulse interaction with the target and the plume[16,51,52] and kT_i from the TOF deconvolution estimates the initial ion temperature. Also, for ns laser ablation at the earlier stage, before ~60 ns, the intense continuum is dominant masking line emission.[10] Since kT_e probed by the OES is time and spatially integrated, it estimates lower temperature than the initial temperature. Thus, for a laser fluence of 21 J/cm^2, the plasma temperature cools from ~6 to below ~1.1 eV from initial plasma expansion until the plasma cools down. With an electric field applied between the target and the grounded mesh, temporal and spatial variations in ion acceleration by the field due to the dynamics of the plasma expansion causes a further spread in the ion velocity not associated with ion plasma temperature. Hence, kT_{ie} represents the combined ion energy spread due to plasma ion temperature and the ion extraction dynamics from the laser plume expending in an external electric field.

IV. CONCLUSION

A combined ion TOF and OES study of laser-generated Al plasma was conducted. The 1064 nm laser ablation source providing 7 ns pulses was operated at a fluence of 21–38 J/cm^2. Production of ions up to Al^{4+} was observed. The energy distributions of the ejected ions were fitted to SCB distribution. The ions are subjected to a Coulomb acceleration proportional to their charge state by the electric field generated at the plasma-vacuum interface of the expanding plume, in addition to the external electric field after their separation from the plasma. The results show significant deviation in the plasma temperature measured by ion energy versus that measured by OES. From the ion TOF measurement, the kT_i increases with the laser fluence from about 6–10 eV for the studied laser fluence range. However, applying the line emission intensity analysis method to OES yields kT_e of about 1.1–1.8 eV. Since the laser plasma is considered at LTE, the present results show that the measurements of kT_e by OES does not reflect the initial high temperature of the plasma in which the ions are produced and the condition of optically thin plasma might not be maintained. Also, the OES data were obtained under temporal and spatial averaging of plasma emission. This averaging also influences the measurements and gives a lower plasma temperature than that achieved in the early part of plume formation, where the plasma is densest and hottest, which are the conditions at which the MCIs are generated. When the plume expands in an applied electric field, ion energy spread, in addition to that due to the plasma ion temperature, is observed due to the interaction of the plume with the external field causing temporal and spatial distortion to the field. Applying voltage to the target had no effect on kT_e as measured by OES.

ACKNOWLEDGMENTS

This material is based upon work supported by the National Science Foundation, USA, under Grant No. MRI-1228228.

[1]R. Janev, L. P. Presnyakov, and V. Shevelko, *Physics of Highly Charged Ions* (Springer Science & Business Media, 2012), Vol. 13.
[2]E. Woryna, P. Parys, J. Wolowski, and W. Mroz, Laser Part. Beams **14**, 293 (1996).
[3]A. Roy, S. S. Harilal, M. P. Polek, S. M. Hassan, A. Endo, and A. Hassanein, Phys. Plasmas **21**, 033109 (2014).
[4]S. Gammino, G. Ciavola, L. Torrisi, L. Celona, J. Wolowski, E. Woryna, P. Parys, L. Laska, J. Krasa, and G. D. Shirkov, Rev. Sci. Instrum. **71**, 1119 (2000).
[5]S. V. Bulanov and V. S. Khoroshkov, Plasma Phys. Rep. **28**, 453 (2002).
[6]V. Y. Fominski, S. N. Grigoriev, R. I. Romanov, A. G. Gnedovets, and P. N. Chernykh, Nucl. Instrum. Methods Phys. Res., Sect. B **313**, 68 (2013).
[7]F. Caridi, L. Torrisi, and L. Giuffrida, Nucl. Instrum. Methods Phys. Res., Sect. B **268**, 499 (2010).
[8]O. Balki and H. E. Elsayed-Ali, Rev. Sci. Instrum. **87**, 113304 (2016).
[9]L. Láska, K. Jungwirth, B. Králiková, J. Krása, M. Pfeifer, K. Rohlena, J. Skála, J. Ullschmied, J. Badziak, P. Parys, J. Wolowski, E. Woryna, S. Gammino, L. Torrisi, F. P. Boody, and H. Hora, Plasma Phys. Controlled Fusion **45**, 585 (2003).
[10]S. S. Harilal, B. O'shay, M. S. Tillack, and M. V. Mathew, J. Appl. Phys. **98**, 013306 (2005).
[11]R. Fabbro, C. Max, and E. Fabre, Phys. Fluids **28**, 1463 (1985).
[12]S. J. Gitomer, R. D. Jones, F. Begay, A. W. Ehler, J. F. Kephart, and R. Kristal, Phys. Fluids **29**, 2679 (1986).
[13]J. I. Apinaniz, B. Sierra, R. Martinez, A. Longarte, C. Redondo, and F. Castano, J. Phys. Chem. C **112**, 16556 (2008).
[14]P. Ecija, M. S. Rayo, R. Martinez, B. Sierra, C. Redondo, F. J. Basterretxea, and F. Castano, Phys. Rev. A **77**, 032904 (2008).
[15]S. Amoruso, M. Armenante, V. Berardi, R. Bruzzese, G. Pica, and R. Velotta, Appl. Surf. Sci. **106**, 507 (1996).
[16]X. Wang, S. Zhang, X. Cheng, E. Zhu, W. Hang, and B. Huang, Spectrochim. Acta B **99**, 101 (2014).
[17]N. M. Bulgakova, A. V. Bulgakov, and O. F. Bobrenok, Phys. Rev. E **62**, 5624 (2000).
[18]D. Mascali, S. Tudisco, N. Gambino, A. Pluchino, A. Anzalone, F. Musumeci, A. Rapisarda, and A. Spitaleri, Europhys. Lett. **100**, 45003 (2012).
[19]R. A. Burdt, Y. Tao, M. S. Tillack, S. Yuspeh, N. M. Shaikh, E. Flaxer, and F. Najmabadi, J. Appl. Phys. **107**, 043303 (2010).
[20]L. Torrisi, F. Caridi, and L. Giuffrida, Nucl. Instrum. Methods Phys. Res., Sect. B **268**, 2285 (2010).
[21]S. S. Harilal, J. Appl. Phys. **102**, 123306 (2007).
[22]Z. Zhang, P. A. VanRompay, J. A. Nees, and P. P. Pronko, J. Appl. Phys. **92**, 2867 (2002).
[23]S. Canulescu, E. Papadopoulou, D. Anglos, T. Lippert, M. J. Montenegro, S. Georgiou, M. Döbeli, and A. Wokaun, Appl. Phys. A **105**, 167 (2011).
[24]B. Toftmann, B. Doggett, C. Budtz-Jørgensen, J. Schou, and J. G. Lunney, J. Appl. Phys. **113**, 083304 (2013).
[25]B. Toftmann and J. Schou, Appl. Phys. A **112**, 197 (2013).
[26]A. M. Elsied, P. K. Diwakar, M. Polek, and A. Hassanein, J. Appl. Phys. **120**, 173104 (2016).
[27]L. Torrisi, F. Caridi, D. Margarone, and A. Borrielli, Nucl. Instrum. Methods Phys. Res., Sect. B **266**, 308 (2008).

[28]J. R. Freeman, S. S. Harilal, B. Verhoff, A. Hassanein, and B. Rice, Plasma Sources Sci. Technol. **21**, 055003 (2012).
[29]M. H. A. Shaim and H. E. Elsayed-Ali, Nucl. Instrum. Methods Phys. Res., Sect. B **356**, 75 (2015).
[30]G. Abdellatif and H. Imam, Spectrochim. Acta B **57**, 1155 (2002).
[31]E. Hontzopoulos, D. Charalambidis, C. Fotakis, G. Farkas, Z. G. Horváth, and C. Toth, Opt. Commun. **67**, 124 (1988).
[32]M. H. A. Shaim, F. G. Wilson, and H. E. Elsayed-Ali, J. Appl. Phys. **121**, 185901 (2017).
[33]J. R. Freeman, S. S. Harilal, P. K. Diwakar, B. Verhoff, and A. Hassanein, Spectrochim. Acta B **87**, 43 (2013).
[34]M. H. A. Shaim and H. E. Elsayed-Ali, Rev. Sci. Instrum. **86**, 073304 (2015).
[35]M. H. A. Shaim, M. M. Rahman, O. Balki, A. Sarkissian, M. L. KorwinPawlowski, and H. E. Elsayed-Ali, Vacuum **137**, 14 (2017).
[36]K. Yamada, T. Tetsuka, and Y. Deguchi, J. Appl. Phys. **69**, 6962 (1991).
[37]S. Gurlui, M. Agop, P. Nica, M. Ziskind, and C. Focsa, Phys. Rev. E **78**, 026405 (2008).
[38]R. Kelly and R. Dreyfus, Surf. Sci. **198**, 263 (1988).
[39]A. Miotello and R. Kelly, Appl. Surf. Sci. **138**, 44 (1999).
[40]A. Lorussoa, J. Krasa, K. Rohlena, V. Nassisi, F. Belloni, and D. Doria, Appl. Phys. Lett. **86**, 081501 (2005).
[41]N. Farid, S. S. Harilal, H. Ding, and A. Hassanein, Phys. Plasmas **20**, 073114 (2013).
[42]R. Teghil, L. d'Alessio, A. Santagata, M. Zaccagnino, D. Ferro, and D. Sordelet, Appl. Surf. Sci. **210**, 307 (2003).
[43]F. F. Chen, Phys. Fluids **25**, 2385 (1982).
[44]S. S. Harilal, C. V. Bindhu, M. S. Tillack, F. Najmabadi, and A. C. Gaeris, J. Appl. Phys. **93**, 2380 (2003).
[45]A. Kramida, Yu. Ralchenko, J. Reader, and NIST ASD Team, see http://physics.nist.gov/asd for NIST Atomic Spectra Database (ver. 5.3) (National Institute of Standards and Technology, Gaithersburg, MD, 2015); accessed 11 July 2017.
[46]H. Griem, *Spectral Line Broadening by Plasmas* (Academic Press, New York, 1974).
[47]L. J. Radziemski, T. R. Loree, D. A. Cremers, and N. M. Hoffman, Anal. Chem. **55**, 1246 (1983).
[48]A. M. El Sherbini, T. M. El Sherbini, H. Hegazy, G. Cristoforetti, S. Legnaioli, V. Palleschi, L. Pardini, A. Salvetti, and E. Tognoni, Spectrochim. Acta B **60**, 1573 (2005).
[49]C. Colon, G. Hatem, E. Verdugo, P. Ruiz, and J. Campos, J. Appl. Phys. **73**, 4752 (1993).
[50]A. W. Allen, M. Blaha, W. W. Jones, A. Sanchez, and H. R. Griem, Phys. Rev. A **11**, 477 (1975).
[51]M. Tillack, D. Blair, and S. Harilal, Nanotechnology **15**, 390 (2004).
[52]S. Amoruso, Appl. Phys. A **69**, 323 (1999).